Application of the Trace Coherence to HH-VV PolInSAR TanDEM-X Data for Vegetation Height Estimation

Noelia Romero-Puig, *Graduate Student Member, IEEE*, Armando Marino, *Member, IEEE*, and Juan M. Lopez-Sanchez, *Senior Member, IEEE*

***Abstract*— This article investigates, for the first time, the inclusion of the operator Trace Coherence (TrCoh) in polarimetric and interferometric synthetic aperture radar (SAR) methodologies for the estimation of biophysical parameters of vegetation. A modified inversion algorithm based on the well-known Random Volume over Ground (RVoG) model, which employs the TrCoh, is described and evaluated. In this regard, a different set of coherence extrema is used as input for the retrieval stage. In addition, the proposed methodology improves the inversion algorithm by employing analytical solutions rather than approximations. Validation is carried out exploiting single-pass HH-VV bistatic TanDEM-X data, together with reference data acquired over a paddy rice area in Spain. The added value of the TrCoh and the convenience of the use of analytical solutions are assessed by comparing with the conventional polarimetric SAR interferometry (PolInSAR) algorithm. Results demonstrate that the modified proposed methodology is computationally more effective than current methods on this dataset. For the same scene, the steps required for inversion are computed in 6 min with the conventional method, while it only takes 6 s with the proposed approach. Moreover, vegetation height estimates exhibit a higher accuracy with the proposed method in all fields under evaluation. The root-mean-squared error reached with the modified method improves by 7 cm with respect to the conventional algorithm.**

***Index Terms*— Agriculture, height, inversion, polarimetric and interferometric synthetic aperture radar (SAR), trace coherence (TrCoh).**

I. Introduction

POLARIMETRIC synthetic aperture radar (SAR) interferometry (PolInSAR) [1] can be used for the retrieval of vegetation parameters, and it often relies on the inversion of physical models, e.g., [2]–[6], among many others. Such physical models are used to relate the PolInSAR measurements (i.e., interferometric complex coherences acquired at different polarimetric channels) to scene biophysical parameters (e.g., vegetation height). In the literature, the most widely used model for this purpose is the Random Volume over Ground (RVoG) [7]–[10].

One of the most critical steps in current RVoG inversion algorithms is the line fit to the coherences represented on a complex plane and the selection of the extreme coherences associated with minimum and maximum ground contributions [11]–[13]. This process requires an understanding of the coherence region (i.e., locus of points in the polar plot), which contains all possible coherence values. A traditional way considers the border of the coherence region and the identification of coherences with extreme phase values. This is the starting point of the inversion algorithm, from which the rest of the model parameters are retrieved [2], [11]–[14]. Consequently, the accuracy of the final estimates is strongly determined by this selection.

In this article, we investigate the use of the operator Trace Coherence (TrCoh), originally derived in [15], as a key part of the PolInSAR inversion strategy for the estimation of vegetation parameters, with a focus on the vegetation height. This operator provides the center of mass of the coherence region, which is the location of maximum accumulation of coherences in the complex plane. This center of mass is calculated by an approximation of the integral of the PolInSAR coherences over all possible scattering mechanisms. Therefore, the TrCoh synthesizes information of the physical target observed by the SAR system as a single entity. Moreover, it represents a coherence independent of the selection of a specific scattering mechanism.

In this work, a modified PolInSAR inversion methodology that employs the TrCoh is proposed for the first time. We use the rationale that, in order to improve the fitting of the data with the model assumptions, the RVoG line needs to cross the point of maximum accumulation of coherences, i.e., the TrCoh. This new line produces a different set of coherence extrema, which is employed as input for inversion. In addition, the proposed methodology refines the conventional PolInSAR inversion algorithm for dual-pol data by introducing analytical solutions, instead of approximations. The complementary information provided by the TrCoh and the convenience of the use of analytical solutions are investigated and assessed to improve current PolInSAR parameter retrieval strategies. Our investigation exploits HH-VV dual-pol TanDEM-X [16] data

Manuscript received April 8, 2021; revised June 7, 2021; accepted July 18, 2021. This work was supported in part by the Spanish Ministry of Science and Innovation, in part by the State Agency of Research (AEI), and in part by the European Funds for Regional Development (EFRD) under Project TEC2017-85244-C2-1-P. The work of Noelia Romero-Puig was supported in part by Generalitat Valenciana and in part by the European Social Fund (ESF) under Grant ACIF/2018/204. *(Corresponding author: Noelia Romero-Puig.)*

Noelia Romero-Puig and Juan M. Lopez-Sanchez are with the Institute for Computer Research (IUII), University of Alicante, 03080 Alicante, Spain (e-mail: noelia.romero@ua.es; juanma-lopez@ieee.org).

Armando Marino is with the Faculty of Natural Sciences, University of Stirling, Stirling FK9 4LA, U.K. (e-mail: armando.marino@stir.ac.uk).

Digital Object Identifier 10.1109/TGRS.2021.3101016

of an area in Seville (Spain), in which ground-truth data over rice fields are available.

This article is organized as follows. Section II provides a theoretical introduction to PolInSAR with the purpose of presenting the mathematical formalism behind the inversion strategy. In Section III, the proposed dual-pol inversion based on the TrCoh is detailed. Then, Section IV describes the test site and the available dataset. In Section V, the results of the inversion methodology are presented and analyzed with the validation data. Finally, Section VI discusses the results and draws the final conclusions.

II. Polarimetric SAR Interferometry

PolInSAR processing exploits the variation of interferometric coherence with polarization to characterize the physical target observed by the radar [1], [10]. In the case of HH-VV dual-pol TanDEM-X data [16], each partial target is expressed as a scattering vector

$$\vec{k}_1 = \left[S^1_{\mathrm{HH}}, \quad S^1_{\mathrm{VV}}\right]^{\mathrm{T}}, \quad \text{and} \quad \vec{k}_2 = \left[S^2_{\mathrm{HH}}, \quad S^2_{\mathrm{VV}}\right]^{\mathrm{T}} \tag{1}$$

where S^n_{PP} represents the complex scattering amplitude at the nth end of the spatial baseline. With partial targets (i.e., targets composed by different scattering mechanisms), we need to extract second-order statistics. Typically, this is described by means of the covariance $[C]$ or coherency $[\mathrm{T}]$ matrix according to a lexicographic or Pauli basis, respectively. Thus, the covariance matrix is defined as

$$[C] = \left\langle \vec{k}_n \cdot \vec{k}_n^{*\mathrm{T}} \right\rangle = \begin{bmatrix} [C_{11}] & [\Omega_{12}] \\ [\Omega_{12}]^{*\mathrm{T}} & [C_{22}] \end{bmatrix} \tag{2}$$

where superscript $*$ denotes the conjugate, T denotes the transposition, and $\langle\cdot\rangle$ denotes spatial averaging or multilooking. In (2), $[C_{11}]$ and $[C_{22}]$ are 2×2 polarimetric matrices, whereas $[\Omega_{12}]$ is a 2×2 matrix containing polarimetric and interferometric information.

To form interferograms, scattering vectors $\vec{k}_1$ and $\vec{k}_2$ are converted into scalars employing unitary complex vectors $\vec{\omega}$, which specifies the selected polarimetric combination, $S_n(\vec{\omega}) = \vec{\omega}^{*\mathrm{T}} \cdot \vec{k}_n$ [1], [11]. The interferometric combination of both scalars results in the PolInSAR coherence

$$\gamma(\vec{\omega}) = \frac{\vec{\omega}^{*\mathrm{T}}[\Omega_{12}]\vec{\omega}}{\sqrt{\left(\vec{\omega}^{*\mathrm{T}}[C_{11}]\vec{\omega}\right)\left(\vec{\omega}^{*\mathrm{T}}[C_{22}]\vec{\omega}\right)}}. \tag{3}$$

The representation in the polar plot of all the possible PolInSAR coherences varying with the projection vector is the coherence region (CoRe) [17], i.e., $\{\gamma(\vec{\omega}), \vec{\omega} \in \mathbb{C}^2, \|\vec{\omega}\| = 1\}$. The estimation of vegetation parameters by means of PolInSAR is based on its geometrical interpretation. A common technique to derive mathematical properties from the CoRe consists of employing a simplified PolInSAR matrix $[A]$ [11], [18], [19], defined as

$$[A] = [C]^{-1/2}[\Omega_{12}][C]^{-1/2}, \text{ with } [C] = ([C_{11}] + [C_{22}])/2. \tag{4}$$

For dual-pol data, the field of values of any 2×2 matrix $[A]$ is an ellipse [20], [21]. Fig. 1 shows an example of this, where different PolInSAR signatures of four selected scenes are observed. From $[A]$, the characteristic parameters of the

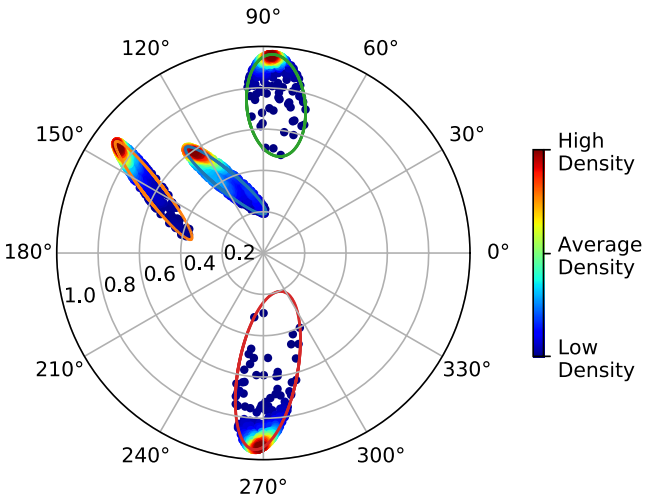

Fig. 1. Unit circle on the complex plane representing the CoRe of four selected scenes with TanDEM-X dual-pol data. Density maps are generated by means of a Monte Carlo simulation [22] of random PolInSAR samples.

CoRe can be obtained by means of a Schur decomposition (see [11, eq. (6.31)])

$$[A] = \begin{bmatrix} a & b \\ c & d \end{bmatrix} \Rightarrow [A] = [U_2]^{*\mathrm{T}} \begin{bmatrix} \lambda_1 & \delta \\ 0 & \lambda_2 \end{bmatrix} [U_2] \tag{5}$$

where

$$\begin{aligned} 2a &= \sqrt{|\lambda_1 - \lambda_2|^2 + |\delta|^2} \\ 2b &= |\delta| \\ g_m &= \frac{1}{2}(\lambda_1 + \lambda_2) \end{aligned} \tag{6}$$

in which λ_1 and λ_2 are the ellipse's foci, a and b are the semimajor and semiminor axis, respectively, and g_m is the center of the ellipse (i.e., mean coherence).

III. Dual-Pol Inversion Based on the Trace Coherence

The proposed inversion algorithm that employs the TrCoh with PolInSAR TanDEM-X data is shown in Fig. 2. The general methodology with TanDEM-X data was first developed for forest scenes in [12]. Then, different methods were proposed to retrieve crop vegetation parameters (e.g., [23]–[25]). Later on, in [13], the RVoG model was adapted for the specific properties of rice scenes (i.e., double-bounce dominant ground contribution). Now, the algorithm is modified according to the inclusion of the TrCoh. To this end, key points of the new algorithm are given as follows.

1) The formulation of the correction of nonvolumetric decorrelation sources [16] for the covariance matrix and the TrCoh is presented for the first time.
2) Due to the elliptical form of the dual-pol CoRe [see (5) and (6)], the analytical expression of the extreme coherences associated with the minimum and maximum ground contributions is derived.
3) A new approach to exploit the TrCoh for vegetation height estimation is proposed.

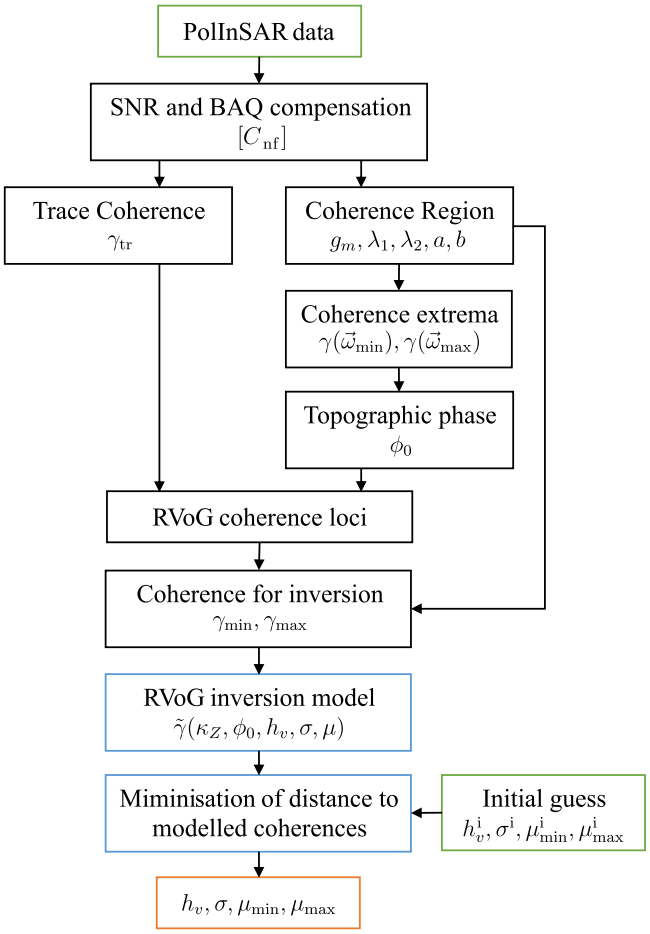

Fig. 2. Proposed RVoG inversion algorithm for PolInSAR TaDEM-X data with application of the TrCoh. The green boxes are the input data, the blue boxes correspond to the parameter retrieval stage, and the orange box corresponds to the output estimates.

4) Given the expressions of the CoRe and the TrCoh, the selection of the new set of coherences employed for inversion is also derived analytically.

Following the block diagram in Fig. 2, each of these key steps is detailed in Sections II-A–II-D.

A. Covariance Denoising

In bistatic TanDEM-X acquisitions, after range spectral filtering [26], the main nonvolumetric decorrelation contribution is due to additive noise, γ_{SNR} [16]. Therefore, each polarization channel needs to be compensated by the signal-to-noise ratio (SNR) decorrelation at pixel level [12]. Then, a remaining nonvolumetric decorrelation term that requires to be compensated as well corresponds to the data quantization effects, γ_{BAQ} [27].

Considering the PolInSAR input data expressed by means of the covariance matrix, the compensation of the SNR decorrelation is performed by directly subtracting the noise from the PolInSAR measurements

$$\begin{aligned}\left[\widehat{C_{11}}\right] &= [C_{11}] - [N_1] \\ \left[\widehat{C_{22}}\right] &= [C_{22}] - [N_2] \\ \left[\widehat{\Omega_{12}}\right] &\equiv [\Omega_{12}]\end{aligned} \tag{7}$$

where $[N_n]$ corresponds to a matrix containing the annotated noise equivalent sigma zero (NESZ) values for the HH and VV channels provided by the standard TanDEM-X products [12]. It is formulated as

$$[N_n] = \begin{bmatrix} \mathrm{NESZ}_{\mathrm{HH}}^n & 0 \\ 0 & \mathrm{NESZ}_{\mathrm{VV}}^n \end{bmatrix} \tag{8}$$

where $n = 1, 2$ denote the master and slave images.

For the SNR (7) correction, in $[\Omega_{12}]$, the noise is assumed to cancel with spatial averaging. This is because the noise is independent of each pixel and zero mean. A coherent sum of zero mean variables is proximal to zero. Thus, there is no way to remove the effect of noise on $[\Omega_{12}]$.

In the second place, the correction of quantization effects is performed as follows:

$$\begin{aligned}[C_{11\,\mathrm{nf}}] &= \left[\widehat{C_{11}}\right] \cdot \gamma_{\mathrm{BAQ}} \\ [C_{22\,\mathrm{nf}}] &= \left[\widehat{C_{22}}\right] \cdot \gamma_{\mathrm{BAQ}} \\ [\Omega_{12\,\mathrm{nf}}] &\equiv [\Omega_{12}].\end{aligned} \tag{9}$$

In the case of the BAQ correction (9), multiplying the decorrelation term, i.e., $\gamma_{\mathrm{BAQ}} \simeq 0.965$, by the $[\widehat{C_{11}}]$ and $[\widehat{C_{22}}]$ matrices is equivalent to divide the coherence in (3) by it, as it is commonly performed [13].

Since the noise removal of the covariance matrix is the starting point of the inversion methodology (see Fig. 2), the remaining parameters necessary for inversion are obtained from the denoised covariance matrix. As demonstrated later in Sections V and VI, this has a direct impact on both the accuracy and the computational efficiency of the algorithm.

B. Trace Coherence Denoising

The main novelty of this article is the use of the TrCoh in the PolInSAR retrieval algorithm. This parameter, as introduced by Marino [15], is defined as

$$\gamma_{\mathrm{tr}} = \frac{\mathrm{Trace}([\Omega_{12}])}{\sqrt{\mathrm{Trace}([C_{11}])\mathrm{Trace}([C_{22}])}} \tag{10}$$

where the operator Trace(.) represents the sum of the diagonal elements of a matrix. As mentioned in Section I, the TrCoh provides an approximation to the center of mass of the CoRe. By integrating over all possible realizations of the CoRe, the TrCoh combines, compacts, and synthesizes a large amount of information about the natural scene. Hence, the TrCoh is a unique PolInSAR parameter with which the entire physical target is characterized on average, without being associated with a specific scattering mechanism (e.g., extreme coherences provided by the minimum and maximum ground contributions). This independence of the selection of the scattering mechanism makes the TrCoh also independent of the polarimetric basis. Therefore, matrices $[C_{11}]$, $[C_{22}]$, and $[\Omega_{12}]$ in (10) may be obtained from the covariance $[C]$ or coherency $[T]$ matrices indistinctly. In the proposed methodology, the noise-free TrCoh, i.e., compensated by SNR and BAQ decorrelation terms, is directly obtained from the denoised covariance matrices (9) using (10).

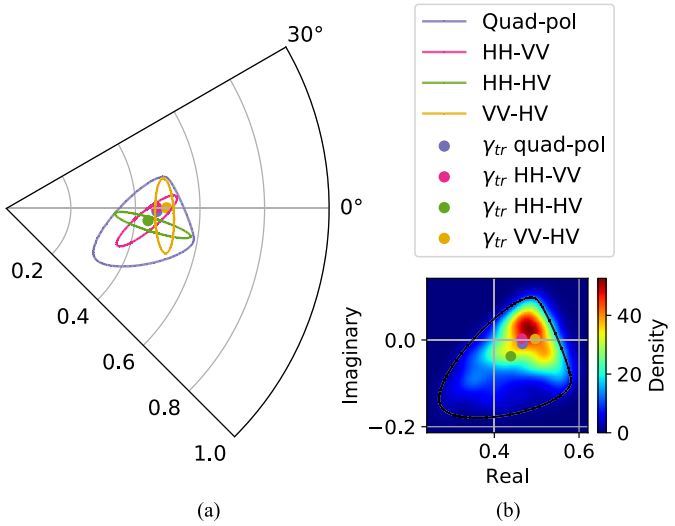

Fig. 3. CoRe and density map of a quad-pol system compared with the equivalent dual-pol CoRe. TrCoh of each polarimetric channel is represented as a colored dot. Data correspond to a maize sample of around 1.8-m height measured at 9 GHz (X-band) in the EMSL, JRC-Ispra. (a) CoRe and TrCoh of the different polarimetric combinations: quad-pol, HH-VV, HH-HV, and VV-HV dual-pol. (b) Density map of a quad-pol system.

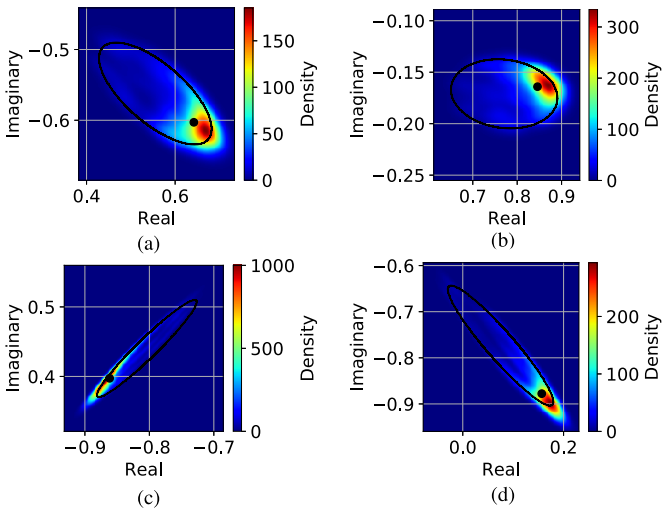

Fig. 4. CoRe and TrCoh (black dot) of four selected scenes with TanDEM-X dual-pol data. Density maps are generated by means of a Monte Carlo simulation [22] of random PolInSAR samples. (a) Wide CoRe with an almost symmetrical distribution of points. (b) Wide CoRe with a nonsymmetrical distribution of points. (c) Narrow CoRe with a nonsymmetrical distribution of points. (d) Narrow CoRe with an almost symmetrical distribution of points.

Alternatively, the denoised TrCoh can be computed independently of the denoised covariance matrix, i.e., directly from the measurements $[C]$. In that case, the compensation of the SNR decorrelation for the TrCoh would be performed based on traces

$$\mathrm{SNR}_1 = \frac{\mathrm{Trace}\left(\left[\widehat{C_{11}}\right]\right)}{\mathrm{Trace}([N_1])}, \quad \mathrm{SNR}_2 = \frac{\mathrm{Trace}\left(\left[\widehat{C_{22}}\right]\right)}{\mathrm{Trace}([N_2])}. \quad (11)$$

Please note that, in (11), the noise of the partial target is not associated with a specific scattering mechanism. γ_{SNR} would be then computed as usual [12]

$$\gamma_{\mathrm{SNR}} = \frac{1}{\sqrt{\left(1+\frac{1}{\mathrm{SNR}_1}\right)\left(1+\frac{1}{\mathrm{SNR}_2}\right)}}. \quad (12)$$

With (12), the noise would be removed from the TrCoh by $\widehat{\gamma_{\mathrm{tr}}} = \gamma_{\mathrm{tr}}/\gamma_{\mathrm{SNR}}$. Finally, the noise free TrCoh would be obtained after compensation of BAQ effects: $\gamma_{\mathrm{tr_{nf}}} = \widehat{\gamma_{\mathrm{tr}}}/\gamma_{\mathrm{BAQ}}$.

In a reduced dual-pol observation space (i.e., TanDEM-X data), the CoRe is contained in an ellipse (6). However, the real CoRe of quad-pol is not bound to be an ellipse. This means that some of the coherence values can only be observed using quad-pol, and the dual-pol CoRe is a subset of the full region. It is obvious that, once dual-pol data are acquired, we are only observing a subregion, and there is no way to know what the full region is. Trying to quantify the differences of dual- and quad-pol regions on different target types is outside the purpose of this work. However, in Fig. 3, we show a preliminary test that suggests that the dual-pol region using HH-VV on crops is a decent approximation of the full region and the best among all the dual-pol combinations on the linear basis. Therefore, we assume that the TrCoh in dual-pol HH-VV data is a good approximation for the TrCoh in quad-pol data over rice fields.

Examples that offer an empirical physical interpretation of the TrCoh with the dual-pol data exploited in this study are shown in Fig. 4. The CoRe and its density map are represented for scenes with different shapes and distribution of points. In all cases, the TrCoh is close to the center of mass of the CoRe. More validation examples about this feature are provided by Marino in [15]. Please note the center of mass is the average of all the possible coherence values, but it is not the mode (i.e., peak) of the density function.

C. Line Fit and Estimation of the Coherence Extrema

A crucial step in the inversion algorithm is the line fit to the CoRe and the identification of the coherence extrema [2]. These coherences are provided by the two scattering mechanisms that maximize the separation of the phase center [1], [11]. Among the different methods to obtain the coherence extrema [28]–[30], this process is usually performed in two steps [12], [13]. First, starting from the coherency matrix, the border of the CoRe is generated by means of an eigenproblem [17]. Then, the extreme coherences with minimum and maximum phases are identified. These coherences correspond to those with minimum and maximum ground contribution, associated with the projection vectors $\vec{\omega}_{\mathrm{min}}$, $\vec{\omega}_{\mathrm{max}}$, respectively. They are the coherences furthest and closest to the topographic phase.

In this article, we propose to obtain the coherence extrema, i.e., the points that maximize the phase separation, from the analytical expression of the coherence loci. For dual-pol data, this corresponds to the locus of points defined by an ellipse in the complex plane, as in (5) and (6). The solution is straightforward. The starting point is the expression of the ellipse (6) in the complex plane. In Cartesian coordinates, $\gamma_{\mathrm{ell}} = x + iy$

$$\begin{aligned} x &= a\cos\phi\cos\theta - b\sin\phi\sin\theta + \Re(g_m) \\ y &= a\sin\phi\cos\theta - b\cos\phi\sin\theta + \Im(g_m) \end{aligned} \quad (13)$$

where a and b are the semimajor and semiminor axes, g_m the center [as in (6)], ϕ the rotation angle, and θ the independent variable. From (13), the phase corresponds to $\varphi = \arctan(y/x)$. Thus, the minimum and maximum phases, i.e., $\varphi_{\min}$ and $\varphi_{\max}$, are provided by the critical angle

$$\theta_c = \pm \arccos\left(\frac{pm - qn}{t}\right) - \arctan(-s/k) \tag{14}$$

in which

$$\begin{aligned} n = a\cos\phi, \quad m = -b\sin\phi, \quad k &= q\Re(g_m) - m\Im(g_m) \\ p = a\sin\phi, \quad q = b\cos\phi, \quad s &= n\Im(g_m) - p\Re(g_m) \\ t &= \operatorname{sgn}(k)\sqrt{k^2 + s^2}. \end{aligned} \tag{15}$$

From (14) and (15), the coherence points of minimum and maximum phase are obtained. These points are the coherence extrema: $\gamma(\vec{\omega}_{\min})$ and $\gamma(\vec{\omega}_{\max})$.

In the end, the line fit to the CoRe is performed by connecting the computed extreme coherences. These two points are of special interest for the estimation of the ground topography, which is computed as in [12]. The intersection of the line defined by the extreme coherences and the unit circle, moving from $\gamma(\vec{\omega}_{\min})$ to $\gamma(\vec{\omega}_{\max})$, provides the estimation of the topographic phase, i.e., ϕ_0.

Fig. 5 shows the difference between the CoRe obtained by means of an approximation [17] and analytically using the expression of the ellipse (6). Although the approximation is usually accurate enough, specific scenes where the difference is noticeable have been selected for illustration purposes.

Fig. 5(a) corroborates that the dual-pol ellipse is distorted when computing it from the approximation. An extreme case is shown in the CoRe on the left, in which the approximated CoRe (i.e., orange dots) shrinks to a straight line, whereas the analytical CoRe (i.e., blue line) remains an ellipse. The approximated CoRe is formed by discrete, not continuous, points. In addition, the distribution of these points is not uniform but more concentrated at the more angular extremes. A consequence of this is represented in Fig. 5(b). While the analytical extreme coherences correspond to the points of minimum and maximum phase, the approximated coherences, located at the area of the low density of points, are slightly different. In this case, the difference between the analytical and approximated solutions leads to an important mismatch in the estimation of the topographic phase. Since the topographic phase is the first parameter to be estimated (see Fig. 2), a bias in its estimation results in a bias in the estimation of the rest of model parameters, i.e., h_v, σ, $\mu_{\min}$, and $\mu_{\max}$.

D. Coherence Loci of the RVoG Model

The RVoG model describes the scene as a two-layer medium comprised of a vegetation layer of randomly oriented scatterers and a second layer of impenetrable ground surface [7]–[10]. While the scattering from the volume is distributed according to a vertical reflectivity function $f(z)$ (e.g., exponential [12]), the scattering from the ground is located at a fixed point z_0. Assuming a dominant direct ground contribution [31],

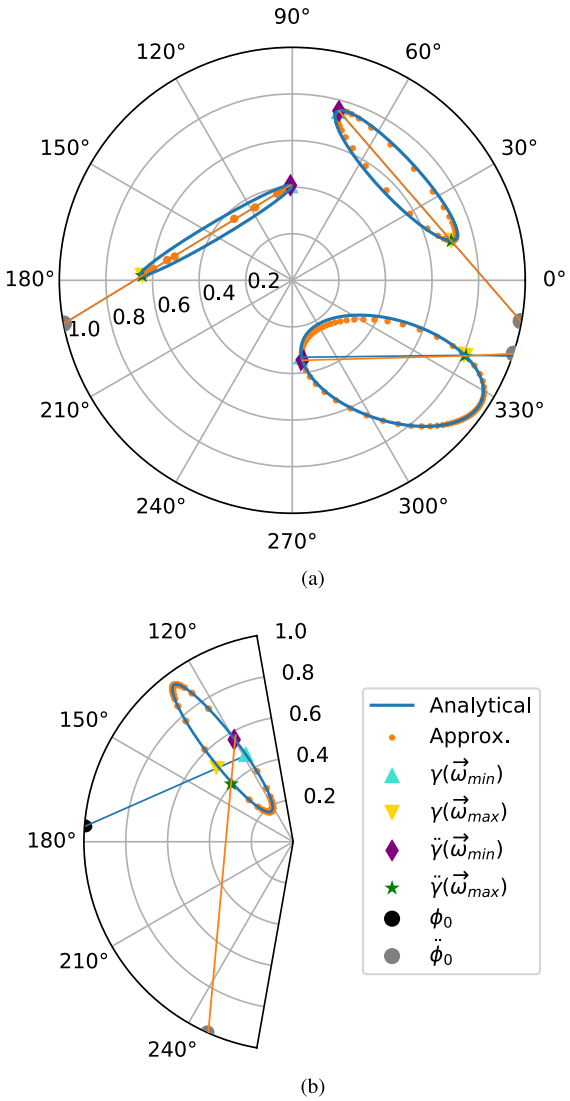

Fig. 5. Comparison of the CoRe (zoomed) obtained by an approximation (blue line) and from the analytical expression (orange dots). Extreme coherences and topographic phase highlighted with two dots are calculated from the approximated CoRe. (a) Distortion of the CoRe computed by approximation. (b) Biased topographic phase obtained from the approximated CoRe.

the PolInSAR coherence can be expressed as follows:

$$\begin{aligned} \tilde{\gamma}(\kappa_Z, \vec{\omega}) &= e^{i\phi_0}\left(\tilde{\gamma}_V + \frac{\mu(\vec{\omega})}{1 + \mu(\vec{\omega})}(1 - \tilde{\gamma}_V)\right) \\ &= e^{i\phi_0}(\tilde{\gamma}_V + F(1 - \tilde{\gamma}_V)) \end{aligned} \tag{16}$$

where κ_Z is the vertical wavenumber that is driven by the effective spatial baseline [7], [8], $\phi_0 = \kappa_Z z_0$ is the topographic phase, and $\tilde{\gamma}_V$ is the coherence of the vegetation volume alone, without any ground contribution. The term $\mu(\vec{\omega})$ is the ground-to-volume ratio at a specific polarization. Thus, the polarization dependence is isolated in a single term F (i.e., with $F \in [0, 1]$). From (16), it is derived that the coherence loci of the RVoG model are a straight line in the complex plane moving along the ground-to-volume amplitude ratio, $\mu(\vec{\omega})$ [9]–[11]. In practice, the visible segment of this line extends from $\gamma(\vec{\omega}_{\min})$ to $\gamma(\vec{\omega}_{\max})$, which are the extreme coherences taken as input for inversion. The use of these two coherence points as input for inversion is justified in the fact

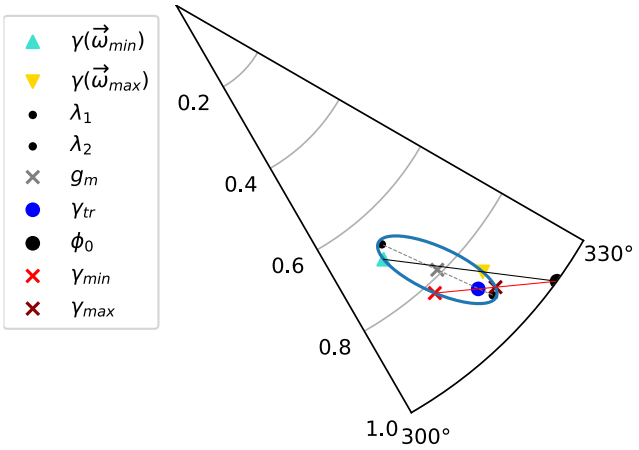

Fig. 6. Dual-pol CoRe and its characteristic parameters of a selected PolInSAR scene.

that they are provided by the scattering mechanisms that yield the largest physical separation in the scene [1], [11].

The methodology proposed in this article not only takes advantage of the information provided by the extreme coherences but it also benefits from the added value provided by the TrCoh. Accordingly, the coherence loci of the RVoG model (16) are redefined as the straight line, which crosses the topographic phase ϕ_0 and the TrCoh γ_{tr}

$$\tilde{\gamma}\left(\kappa_Z, \vec{\omega}\right) = e^{i\phi_0} + F\left(\gamma_{\text{tr}} - e^{i\phi_0}\right). \tag{17}$$

Hence, the coherences taken as input for inversion correspond to the crossings of the redefined RVoG line (17) with the ellipse, which represents the border of the CoRe. Expressing the ellipse (6) as

$$|\gamma - \lambda_1| + |\gamma - \lambda_2| = 2a \tag{18}$$

the system of equations formed by (17) and (18) is solved through the following quadratic equation:

$$AF^2 + BF + C = 0 \;\Rightarrow\; F = \frac{-B \pm \sqrt{B^2 - 4AC}}{2A}$$

with

$$\begin{aligned} A &= 4\left(t_2^2 - 4a^2|\gamma_1 - \gamma_2|^2\right) \\ B &= 4\big[t_1 t_2 - 8a^2(\Re(\gamma_1 - \lambda_2)\Re(\gamma_2 - \gamma_1) \\ &\qquad + \Im(\gamma_1 - \lambda_2)\Im(\gamma_2 - \gamma_1))\big] \\ C &= t_1^2 - 16a^2|\gamma_1 - \lambda_2|^2 \end{aligned}$$

and

$$\begin{aligned} t_1 &= |\gamma_1 - \lambda_1|^2 - |\gamma_1 - \lambda_2|^2 - 4a^2 \\ t_2 &= \Re(\gamma_2 - \gamma_1)\Re(\lambda_2 - \lambda_1) + \Im(\gamma_2 - \gamma_1)\Im(\lambda_2 - \lambda_1). \end{aligned} \tag{19}$$

In (19), $\gamma_1 = e^{i\phi_0}$ and $\gamma_2 = \gamma_{\text{tr}}$. The crossings γ_{min} and γ_{max} are obtained substituting the term F in (17). This new set of coherences is employed for inversion.

Fig. 6 shows the CoRe of a selected scene with its characteristic parameters. The traditional RVoG coherence loci as a straight line defined by the extreme coherences and the topographic phase (in black) are compared with the redefined line crossing the TrCoh (in red). Although we can get different shapes and orientations of the CoRe depending on the physical properties of the volume and the underlying ground for real data [9] (as demonstrated in Fig. 1), the results shown here are very representative. The new coherences taken as input for inversion, γ_{min} and γ_{max}, are consistently of higher magnitude compared to those provided by the extreme phases, i.e., $\gamma\left(\vec{\omega}_{\text{min}}\right)$ and $\gamma\left(\vec{\omega}_{\text{max}}\right)$. In principle, higher coherence magnitude translates into more accurate estimates. This supports the use of the new set of coherences for inversion.

At the end, the numerical inversion of the RVoG model is carried out by an iterative minimization of the distance between the measured complex coherences, i.e., γ_{min} and γ_{max}, and the modeled ones (16) [13]

$$\min_{h_v, \sigma, \mu_{\text{max}}, \mu_{\text{min}}} \left\| \begin{bmatrix} \gamma_{\text{max}} e^{-i\phi_0} \\ \gamma_{\text{min}} e^{-i\phi_0} \end{bmatrix} - \begin{bmatrix} \tilde{\gamma}\left(\kappa_Z, h_v, \sigma, \mu_{\text{max}}\right) \\ \tilde{\gamma}\left(\kappa_Z, h_v, \sigma, \mu_{\text{min}}\right) \end{bmatrix} \right\|. \tag{20}$$

This process yields the final vegetation estimates, i.e., h_v, σ, μ_{min}, and μ_{max}.

E. Interpretation of the Data and the RVoG Model

This section provides additional considerations to help understand the interpretation of the data (i.e., measurements) and the RVoG model (i.e., actual physical scene).

As described in Section III-D, the RVoG model is employed to provide an analytical expression of the interferometric coherence as a function of some physical parameters of the natural scene observed by the radar. It can be shown analytically that the coherence loci of the RVoG model follow a straight line in the complex plane (16). This line follows a physical criterion by definition. The aim of the inversion is to find out how to extract the RVoG line from the (measured) data available. Nevertheless, at the moment of extracting that line, there exist different options.

One possibility consists of defining the RVoG line as that which crosses the measured coherence points with maximum phase separation [12]. This criterion assumes that these coherences are associated with the highest and lowest scattering centers of the scene along the vertical coordinate. Following this criterion, and moving along the RVoG line, the point with maximum ground contribution (i.e., $\mu \to \infty$) is assumed to be the topographic phase. However, the criterion to retrieve the line from the data could be different. It could be based on maximizing either the coherence magnitude (see [11, Secs. 6.2.1 and 6.2.2]) or the geometrical separation of the coherences (see [11, Sec. 6.2.3]). In that case, with dual-pol data, the maximum separation is given by the major axis of the ellipse. Another possible criterion could be to exploit directly the coherences of the measured polarimetric channels (i.e., γ_{HH} and γ_{VV}) [9]. All these strategies provide different inversion results.

An additional proof of this is the methodology proposed in this article, in which the RVoG line is defined by the TrCoh and the topographic phase (17). The coherence points employed for inversion are then the crossings of that line and the elliptical CoRe.

The key point is that the interpretation of the actual RVoG line is independent of the polarimetric mode used. That is, it is independent of the subspace observed by the available

TABLE I
TANDEM-X SYSTEM PARAMETERS AND ACQUISITION DATES OF THE DATASETS OVER SEVILLE

Incidence angle	HoA [m]	κ_Z [rad/m]	Date range	Day of Year (DoY)
22.7 degrees	2.53	2.48	2015.06.04–08.31	155–243
30 degrees	3.49	1.80	2015.05.04–09.02	124–245
39 degrees	5.81	1.08	2015.05.30–08.26	150–238

polarization channels in dual-pol. In other words, while the CoRe depends on the type of polarimetric data acquired (as shown in Fig. 3), the RVoG model represents the physical scene, which is the same regardless of the subspace measured by the dual-pol mode. Fig. 3 not only highlights the limits of a dual-pol observation with respect to quad-pol but also manifests the independence of the RVoG model with respect to the subspace observed by the dual-pol mode. Following, e.g., the criterion of maximum phase separation, the observed CoRe from different dual-pol combinations leads to different estimates of the topographic phase and, thus, to different estimates of the remaining model parameters. This supports the use of the TrCoh in defining the inversion methodology. In Fig. 3, we can observe that the center of mass for dual co-pol and quad-pol is very close to each other. This allows us a way to retrieve some information that is similar to the full space and, therefore, more similar to reality. Thus, the TrCoh is the point that best describes the physical target.

IV. TEST SITE AND DATASET

A. Test Site and Ground Campaign Data

An area of rice fields is selected for the evaluation of crop height estimates. The test site, as shown in Fig. 7, covers an area of 30 km × 30 km located in Seville, southwest (SW) of Spain (37.1° N, 6.15° W). As opposed to other cultivation practices [32], [33], the parcels are kept flooded during the whole rice growth cycle (from May to October) and not only in the early vegetative stage.

In 2015, the local association of rice farmers gathered agricultural descriptors of four rice fields on a weekly basis. This includes phenological information according to the BBCH (*Biologische Bundesanstalt, Bundessortenamt und CHemische Industrie*) [34] scale and above-water vegetation height. This study area has been widely employed for rice crop monitoring in former studies, e.g., [31]–[37].

B. TanDEM-X Data and SAR Processing

Dual-pol TanDEM-X SAR data acquired during the Science Phase of this mission are exploited. The data cover most of the phenological cycle of the monitored crops, from May to September 2015. Specific characteristics of the employed time series are summarized in Table I. On account of the correlation between the incidence angle (θ_0) and the height of ambiguity (HoA) [38], each time series provides a different level of interferometric sensitivity to the vertical distribution of scatterers within the vegetation volume.

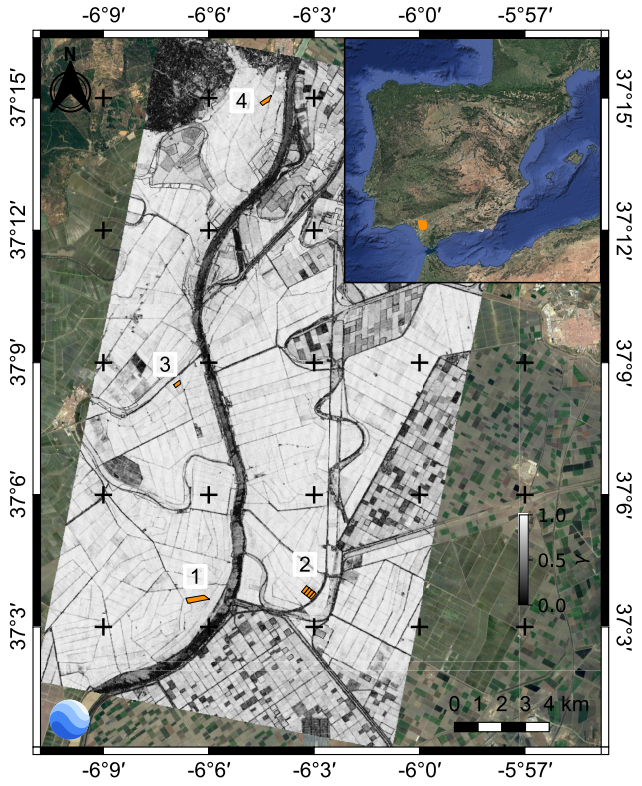

Fig. 7. Coherence amplitude of the HH channel acquired on June 26, 2015, showing the location of the study area in Seville, Spain. The test fields of the ground campaign are highlighted in orange.

The SAR data processing starts from the standard Coregistered Single-Look Slant-range Complex (CoSSC) product of each acquisition. The large spatial baselines that characterize the input data (i.e., 2–3 km) lead to a notable geometrical decorrelation derived from changes in the wavenumber. Hence, range spectral filtering is applied to compensate for this decorrelation. Multilooking is then performed by means of a 21 × 21 boxcar filter. Flat earth and topographic phase contributions are removed before forming the interferograms, so they are actually differential interferograms. In this case, a 5-m grid size DEM provided by the Spanish National Centre for Geographic Information (CNIG) is used in the processing.

V. RESULTS

This section presents the results of the proposed methodology, with a focus on vegetation height. The assessment is performed by comparing these results to those obtained following the conventional PolInSAR method [12], [13]. Fig. 8 shows the temporal evolution of the vegetation height at four monitored fields for 22.7° of incidence. The available time series at this incidence angle is especially suitable for crop monitoring since, as represented in Table I, it is associated with the largest κ_Z and the shortest HoA, i.e., =2.48 rad/m and 2.53 m, respectively. This ensures the highest interferometric sensitivity of the entire dataset. In Fig. 8, the accuracy of the vegetation height estimates of the PolInSAR conventional method (denoted as $M1$, in red) and the proposed one (denoted as $M2$, in green) is analyzed by direct comparison with the reference ground-truth data (in black). Although both

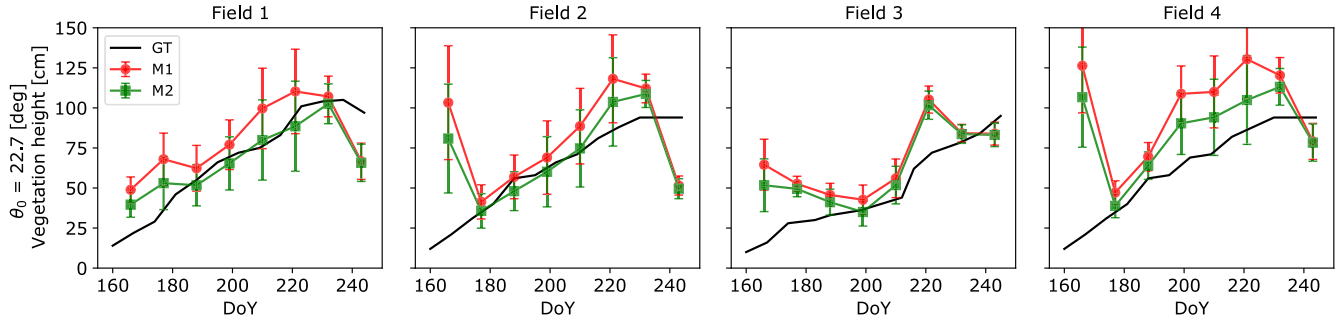

Fig. 8. Temporal evolution of the vegetation height. Estimates obtained following the conventional PolInSAR method (red) are compared with estimates obtained with the proposed approach (green) and with the ground-truth data (black). Columns from left to right show estimates of the four monitored rice fields in Seville, for an incidence of 22.7°. Average results computed for all pixels inside each field are presented. Error bars denote standard deviation.

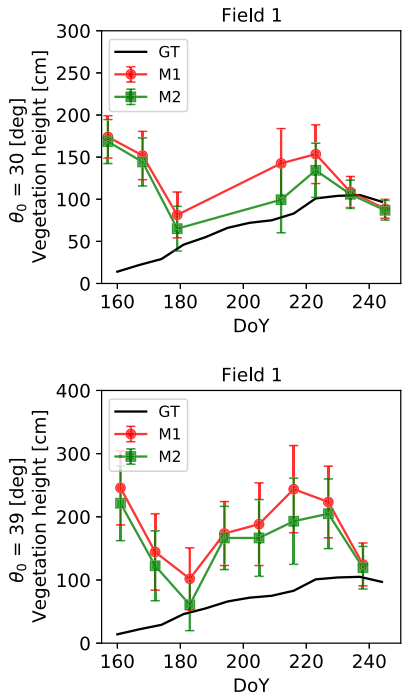

Fig. 9. Temporal evolution of the vegetation height: Field 1. Estimates obtained following the conventional PolInSAR method (red) are compared with estimates obtained with the proposed approach (green) and with the ground-truth data (black). Results are presented for an incidence of (Top) 30° and (Bottom) 39°. Average results computed for all pixels inside each field are presented. Error bars denote standard deviation.

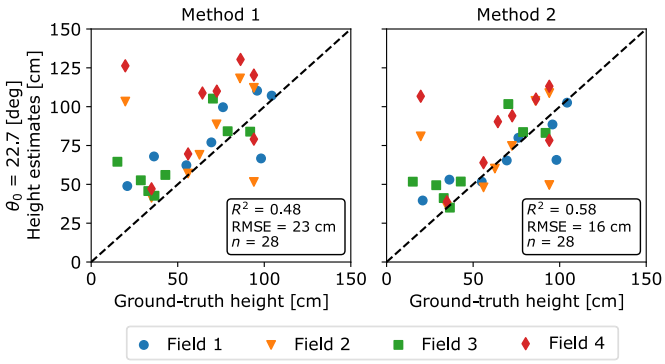

Fig. 10. Correlation plots of the vegetation height estimates with respect to the ground-truth data. Method 1 corresponds to the conventional RVoG inversion, whereas Method 2 corresponds to the proposed approach. Statistics are computed for the range of values in which field measurements are above 25 cm (i.e., from the second available TanDEM-X acquisition onward).

methodologies perform relatively well, estimates obtained with the proposed approach based on the TrCoh are closer to the reference data in all cases.

Focusing now on a single field, Field 1, Fig. 9 shows the temporal evolution of the vegetation height for incidences of 30° (top) and 39° (bottom). Similar results as those in Fig. 8 are observed. Vegetation height estimates retrieved with the proposed approach are more accurate than those of the conventional method. Nevertheless, as one moves to shallower incidences, the improvement seems less noticeable. Hence, at 39°, a clear overestimation is still present at most dates, even with the proposed method. Although not shown here, analogous results are obtained for the remaining fields.

Common behavior in both methodologies is that, at the early season (DoY $<$ 180), when plants are very small (i.e., below ~30 cm), there is a lack of interferometric sensitivity to the vertical distribution of scatterers in the scene, which leads to overestimated vegetation heights [11], [13], [33]. The flooded ground reflects the incident signal in a specular direction, yielding low returns to the SAR antenna. At 22.7°, the overestimation is mainly restricted to the first dates. However, at 30° and 39°, due to the associated large HoA and reduced vertical wavenumber (see Table I), this effect is visible through the entire crop season. This explains the overestimation observed at these shallower incidences.

A quantitative comparison between average inversion height per field and date against ground-truth data is presented in Fig. 10. Previous comments on the trends observed in the estimated heights can also apply to the results in Fig. 10. For very short vegetation, a lack of interferometric sensitivity together with small residual nonvolumetric decorrelation yields important height errors. Due to the very low signal returns at these dates, even after the compensation of the coherence, i.e., by SNR and BAQ corrections (see Sections III-A and III-B), the signal levels are still not enough to ensure a reliable inversion. Hence, there will always be some decorrelation that cannot be compensated for. On this basis, larger effective spatial baselines than the ones provided in the current dataset (see Table I) should be used to provide suitable short vegetation height estimates. In accordance with this criterion, statistics presented in Fig. 10 are computed

for the range of values in which field measurements are above 25 cm (i.e., from the second available TanDEM-X acquisition onward). Thus, the analysis is performed over $n = 28$ measurements. A root-mean-squared error (RMSE) of 23 cm and a determination coefficient R^2 of 0.48 are obtained with the conventional PolInSAR method. On the other hand, an RMSE of 16 cm and an R^2 of 0.58 are achieved with the proposed approach. Again, these numbers refer to rice plants taller than 25 cm.

VI. Conclusion and Discussion

This article presents a modified PolInSAR inversion methodology based on the operator TrCoh. Key points of the proposed inversion methodology are reviewed to evaluate the added value of the TrCoh and the benefits of the use of analytical solutions.

1) The formulation of the correction of nonvolumetric decorrelation sources of the covariance matrix and the TrCoh leads to a direct and simple application. Higher coherences provide lower overestimation.
2) The exploitation of the elliptical form of the dual-pol CoRe for the computation of the coherence extrema speeds up the inversion and provides more accurate results not based on approximations.
3) The inclusion of the TrCoh in the PolInSAR retrieval algorithm is analyzed for the first time. As a result, the coherence loci of the RVoG model are forced to cross the TrCoh. This produces a line, which is more stable, since it is more related to the bulk of the distribution of coherence in the polar plot.
4) Due to the expressions of the CoRe and the TrCoh, the analytical selection of the new set of coherences used for inversion is faster than other methods based on approximations [17].

The suitability of using the TrCoh for inversion is justified in improved accuracy of the resulting vegetation height estimates. An RMSE of 16 cm is obtained with the proposed method, which is an improvement of 7 cm with respect to the conventional PolInSAR method. Regarding the coefficient R^2, the accuracy improves by 10% with the proposed approach. We interpret that this is because we constrain the line to pass through the area of most points in the CoRe (capturing more of the target). At the same time, this justifies why we obtain more accurate results with the TrCoh than following other criteria based only on the CoRe, such as employing the vertices of the major axis of the ellipse for inversion. Although not included here, results following this latter approach are far worse than those based on the TrCoh (or on the maximum phase separation, such as the conventional PolInSAR method). This leads us to conclude that the selection of the measured coherences employed for inversion, as modeled by the RVoG, needs to focus on the most significant representation of the physical target, which is not represented by the dual-pol ellipse axes.

In addition, the use of analytical solutions enhances computational efficiency. A 16 cores computer with 160-GB RAM and a scene of 1500 $\times$ 300 pixels corresponding to Field 1 (e.g., on June 15) are considered to quantify the improvement. Since the minimization is a common step (see Fig. 2), the comparison between the conventional and the proposed method is performed without considering this final stage. Thus, the conventional algorithm, with $N = 72$ points to simulate the CoRe, takes around 6 min and 4 s, whereas the same required steps with the proposed approach are performed in 6 s. As the number of points used in the conventional method to approximate the CoRe increases, so does the computational cost. For instance, employing $N = 720$ points would be required to avoid important mismatches, as the one observed in Fig. 5(b). Such a larger number can help prevent the important bias observed in the extreme coherences computed with the approximate method. The density of points of the approximated border of the CoRe would be higher, and thus, the approximated extreme coherences would be closer to their actual values. In that case, the computational cost increases up to 8 min.

Overall, the modified PolInSAR parameter retrieval strategy based on the TrCoh yields more accurate height estimates in a more efficient and analytical manner. Moreover, the methodology presented here can apply to other scenarios, e.g., crops with nonflooded ground conditions or forest scenes.

Acknowledgment

All the TanDEM-X data were provided by the German Aerospace Center (DLR) under project NTI-POLI6736. The authors would also like to thank the support of the Federación de Arroceros de Sevilla for providing the field data.

References

[1] S. R. Cloude and K. P. Papathanassiou, "Polarimetric SAR interferometry," *IEEE Trans. Geosci. Remote Sens.*, vol. 36, no. 5, pp. 1551–1565, Sep. 1998.
[2] F. Kugler, S.-K. Lee, I. Hajnsek, and K. P. Papathanassiou, "Forest height estimation by means of Pol-InSAR data inversion: The role of the vertical wavenumber," *IEEE Trans. Geosci. Remote Sens.*, vol. 53, no. 10, pp. 5294–5311, Oct. 2015.
[3] H. Chen, S. R. Cloude, D. G. Goodenough, D. A. Hill, and A. Nesdoly, "Radar forest height estimation in mountainous terrain using Tandem-X coherence data," *IEEE J. Sel. Topics Appl. Earth Observ. Remote Sens.*, vol. 11, no. 10, pp. 3443–3452, Oct. 2018.
[4] M. Denbina, M. Simard, and B. Hawkins, "Forest height estimation using multibaseline PolInSAR and sparse lidar data fusion," *IEEE J. Sel. Topics Appl. Earth Observ. Remote Sens.*, vol. 11, no. 10, pp. 3415–3433, Oct. 2018.
[5] Y. Xie, H. Fu, J. Zhu, C. Wang, and Q. Xie, "A LiDAR-aided multibaseline PolInSAR method for forest height estimation: With emphasis on dual-baseline selection," *IEEE Geosci. Remote Sens. Lett.*, vol. 17, no. 10, pp. 1807–1811, Oct. 2020.
[6] M. Pichierri, I. Hajnsek, S. Zwieback, and B. Rabus, "On the potential of polarimetric SAR interferometry to characterize the biomass, moisture and structure of agricultural crops at L-, C- and X-bands," *Remote Sens. Environ.*, vol. 204, pp. 596–616, Jan. 2018.
[7] R. N. Treuhaft, S. N. Madsen, M. Moghaddam, and J. J. van Zyl, "Vegetation characteristics and underlying topography from interferometric radar," *Radio Sci.*, vol. 31, no. 6, pp. 1449–1485, Nov. 1996.
[8] R. N. Treuhaft and P. Siqueira, "Vertical structure of vegetated land surfaces from interferometric and polarimetric radar," *Radio Sci.*, vol. 35, no. 1, pp. 141–177, Jan. 2000.
[9] K. P. Papathanassiou and S. R. Cloude, "Single-baseline polarimetric SAR interferometry," *IEEE Trans. Geosci. Remote Sens.*, vol. 39, no. 11, pp. 2352–2363, Nov. 2001.
[10] S. R. Cloude and K. P. Papathanassiou, "Three-stage inversion process for polarimetric SAR interferometry," *IEE Proc.-Radar, Sonar Navigat.*, vol. 150, no. 3, pp. 125–134, Jun. 2003.

[11] S. R. Cloude, *Polarisation: Applications in Remote Sensing*. Oxford, U.K.: Oxford Univ. Press, 2009.
[12] F. Kugler, D. Schulze, I. Hajnsek, H. Pretzsch, and K. P. Papathanassiou, "TanDEM-X Pol-InSAR performance for forest height estimation," *IEEE Trans. Geosci. Remote Sens.*, vol. 52, no. 10, pp. 6404–6422, Oct. 2014.
[13] J. M. Lopez-Sanchez, F. Vicente-Guijalba, E. Erten, M. Campos-Taberner, and F. J. Garcia-Haro, "Retrieval of vegetation height in rice fields using polarimetric SAR interferometry with TanDEM-X data," *Remote Sens. Environ.*, vol. 192, pp. 30–44, Apr. 2017.
[14] S.-K. Lee and T. E. Fatoyinbo, "TanDEM-X Pol-InSAR inversion for mangrove canopy height estimation," *IEEE J. Sel. Topics Appl. Earth Observ. Remote Sens.*, vol. 8, no. 7, pp. 3608–3618, Jul. 2015.
[15] A. Marino, "Trace coherence: A new operator for polarimetric and interferometric SAR images," *IEEE Trans. Geosci. Remote Sens.*, vol. 55, no. 4, pp. 2326–2339, Apr. 2017.
[16] G. Krieger *et al.*, "TanDEM-X: A satellite formation for high-resolution SAR interferometry," *IEEE Trans. Geosci. Remote Sens.*, vol. 45, no. 11, pp. 3317–3341, Nov. 2007.
[17] T. Flynn, M. Tabb, and R. Carande, "Coherence region shape extraction for vegetation parameter estimation in polarimetric SAR interferometry," in *Proc. IEEE Int. Geosci. Remote Sens. Symp.*, vol. 5, Jun. 2002, pp. 2596–2598.
[18] H. Chen, S. R. Cloude, and D. G. Goodenough, "Forest canopy height estimation using Tandem-X coherence data," *IEEE J. Sel. Topics Appl. Earth Observ. Remote Sens.*, vol. 9, no. 7, pp. 3177–3188, Jul. 2016.
[19] G. Brigot, M. Simard, E. Colin-Koeniguer, and A. Boulch, "Retrieval of forest vertical structure from PolInSAR Data by machine learning using LIDAR-Derived features," *Remote Sens.*, vol. 11, no. 4, p. 381, 2019.
[20] F. D. Murnaghan, "On the field of values of a square matrix," *Proc. Nat. Acad. Sci. USA*, vol. 18, no. 3, pp. 246–248, Mar. 1932.
[21] D. S. Keeler, L. Rodman, and I. M. Spitkovsky, "The numerical range of 3×3 matrices," *Linear Algebra Appl.*, vol. 252, pp. 115–139, Feb. 1997.
[22] J.-S. Lee and E. Pottier, *Polarimetric Radar Imaging: From basics to Applications, of Optical Science and Engineering*, vol. 143. Boca Raton, FL, USA: CRC Press, Feb. 2009.
[23] M. Pichierri and I. Hajnsek, "Comparing performances of crop height inversion schemes from multifrequency pol-InSAR data," *IEEE J. Sel. Topics Appl. Earth Observ. Remote Sens.*, vol. 10, no. 5, pp. 1727–1741, May 2017.
[24] E. Erten, J. M. Lopez-Sanchez, O. Yuzugullu, and I. Hajnsek, "Retrieval of agricultural crop height from space: A comparison of SAR techniques," *Remote Sens. Environ.*, vol. 187, pp. 130–144, Dec. 2016.
[25] O. Yuzugullu, E. Erten, and I. Hajnsek, "Assessment of paddy rice height: Sequential inversion of coherent and incoherent models," *IEEE J. Sel. Topics Appl. Earth Observ. Remote Sens.*, vol. 11, no. 9, pp. 3001–3013, Sep. 2018.
[26] F. Gatelli, A. M. Guamieri, F. Parizzi, P. Pasquali, C. Prati, and F. Rocca, "The wavenumber shift in SAR interferometry," *IEEE Trans. Geosci. Remote Sens.*, vol. 32, no. 4, pp. 855–865, Jul. 1994.
[27] M. Martone, B. Bräutigam, and G. Krieger, "Quantization effects in TanDEM-X data," *IEEE Trans. Geosci. Remote Sens.*, vol. 53, no. 2, pp. 583–597, Feb. 2015.
[28] M. Tabb and R. Carande, "Robust inversion of vegetation structure parameters from low-frequency, polarimetric interferometric SAR," in *Proc. IEEE Int. Geosci. Remote Sens. Symp.*, vol. 7, Jul. 2001, pp. 3188–3190.
[29] R. Fomena and S. Cloude, "On the role of coherence optimization in polarimetric SAR interferometry," in *Proc. CEOS SAR Cal/Val Work.*, Adelaide, NSW, Australia, 2005, pp. 1–6.
[30] L. Ferro-Famil, M. Neumann, and Y. Huang, "Multi-baseline POL-inSAR statistical techniques for the characterization of distributed media," in *Proc. IEEE Int. Geosci. Remote Sens. Symp.*, vol. 3, Jul. 2009, pp. III-971–III-974.
[31] N. Romero-Puig, J. M. Lopez-Sanchez, and J. D. Ballester-Berman, "Estimation of RVoG scene parameters by means of PolInSAR with TanDEM-X data: Effect of the double-bounce contribution," *IEEE Trans. Geosci. Remote Sens.*, vol. 58, no. 10, pp. 7283–7304, Oct. 2020.
[32] C. Rossi and E. Erten, "Paddy-Rice monitoring using TanDEM-X," *IEEE Trans. Geosci. Remote Sens.*, vol. 53, no. 2, pp. 900–910, Feb. 2015.
[33] S.-K. Lee, S. Yoon, and J.-S. Won, "Vegetation height estimate in rice fields using single polarization TanDEM-X science phase data," *Remote Sens.*, vol. 10, no. 11, p. 1702, Oct. 2018.
[34] P. D. Lancashire *et al.*, "A uniform decimal code for growth stages of crops and weeds," *Ann. Appl. Biol.*, vol. 119, no. 3, pp. 561–601, Dec. 1991.
[35] O. Yuzugullu, E. Erten, and I. Hajnsek, "Rice growth monitoring by means of X-band co-polar SAR: Feature clustering and BBCH scale," *IEEE Geosci. Remote Sens. Lett.*, vol. 12, no. 6, pp. 1218–1222, Jun. 2015.
[36] C. Küçük, G. Taşkın, and E. Erten, "Paddy-rice phenology classification based on machine-learning methods using multitemporal co-polar X-band SAR images," *IEEE J. Sel. Topics Appl. Earth Observ. Remote Sens.*, vol. 9, no. 6, pp. 2509–2519, Jun. 2016.
[37] J. M. Lopez-Sanchez, F. Vicente-Guijalba, J. D. Ballester-Berman, and S. R. Cloude, "Influence of incidence angle on the coherent copolar polarimetric response of rice at X-band," *IEEE Geosci. Remote Sens. Lett.*, vol. 12, no. 2, pp. 249–253, Feb. 2015.
[38] J. M. Lopez-Sanchez, F. Vicente-Guijalba, A. Mestre-Quereda, N. Romero, and E. Erten, "Influence of incidence angle and baseline on the retrieval of biophysical parameters of rice fields by means of polarimetric SAR interferometry with TanDEM-X data," in *Proc. IEEE Int. Geosci. Remote Sens. Symp. (IGARSS)*, Jul. 2017, pp. 926–929.

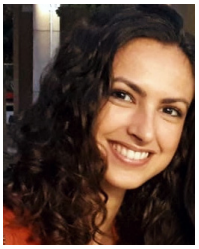

Noelia Romero-Puig (Graduate Student Member, IEEE) received the B.Sc. degree in sound and image in telecommunications engineering and the M.Sc. degree in telecommunication engineering from the University of Alicante, Alicante, Spain, in 2016 and 2018, respectively, where she is currently pursuing the Ph.D. degree with the Signals, Systems and Telecommunication Group.

Her research interests include monitoring agricultural crops by means of SAR interferometry (InSAR) and polarimetric SAR interferometry (PolInSAR) techniques.

Ms. Romero-Puig was a recipient of the Award for Best Final Master's Project in Remote Sensing defended in Spain in 2018 of the IEEE GRSS Spanish Chapter and the Hisdesat Award for the Best Final Master's Project in Government Satellite Services by the Official College of Telecommunications Engineers (COIT).

Armando Marino (Member, IEEE) received the M.Sc. degree in telecommunication engineering from the Università di Napoli "Federico II," Naples, Italy, in 2006, and the Ph.D. degree in polarimetric SAR interferometry from the School of Geosciences, The University of Edinburgh, Edinburgh, U.K., in 2011.

In 2006, he joined the High Frequency and Radar Systems Department, German Aerospace Centre, Weßling, Germany, where he developed his M.Sc. thesis. From March 2011 to October 2011, he was with the Institute of Computing Research, University of Alicante, Alicante, Spain. From December 2011 to May 2015, he was a Post-Doctoral Researcher and Lecturer with the Institute of Environmental Engineering, ETH Zürich, Zürich, Switzerland. Since June 2015, he has been a Lecturer with the School of Engineering and Innovation, The Open University, Milton Keynes, U.K. Since May 2018, he has been a Senior Lecturer (Assistant Professor) with the Faculty of Natural Sciences, University of Stirling, Stirling, U.K.

Juan M. Lopez-Sanchez (Senior Member, IEEE) was born in Alicante, Spain, in 1972. He received the Ingeniero (M.S.) and Doctor Ingeniero (Ph.D.) degrees in telecommunication engineering from the Technical University of Valencia (UPV), Valencia, Spain, in 1996 and 2000, respectively.

From 1998 to 1999, he was a Pre-Doctoral Grantholder with the Space Applications Institute, Joint Research Centre of the European Commission, Ispra, Italy. Since 2000, he has been leading the Signals, Systems and Telecommunication Group, University of Alicante, Alicante, Spain, where he has been a Full Professor since November 2011. He has coauthored more than 80 articles in refereed journals and more than 130 articles and presentations in international conferences and symposia. His main research interests include microwave remote sensing for inversion of biophysical parameters, polarimetric and interferometric techniques, and applications of radar remote sensing in agriculture and geophysics.

Dr. Lopez-Sanchez received the Indra Award for the best Ph.D. thesis about radar in Spain in 2001. From 2006 to 2012, he was the Chair of the Spanish Chapter of the IEEE Geoscience and Remote Sensing Society.